Indonesian Journal of Electrical Engineering and Computer Science
Vol. 41, No. 1, January 2026, pp. 140~152
ISSN: 2502-4752, DOI: 10.11591/ijeecs.v41.i1.pp140-152

Ultra-high isolation dual-port circular patch antenna at 2.4 GHz

Meriem Boucif, Fayza Bousalah, Hayat Benosman
Department of Telecommunication, Laboratory of Telecommunication, Faculty of Technology, University of Tlemcen, Tlemcen, Algeria

Article Info

Article history:

Received Oct 6, 2025
Revised Nov 28, 2025
Accepted Dec 2, 2025

Keywords:

2.4 GHz ISM band
Circular microstrip patch antenna
Defected ground structure
High isolation
MIMO

ABSTRACT

Reliable wireless communication in the 2.4 GHz industrial, scientific, and medical band increasingly relies on antenna systems that can provide high inter-port isolation in multiple-input multiple-output (MIMO) configurations. This paper presents a circular microstrip patch antenna and its extension to a dual-port MIMO configuration designed for 2.4 GHz operation. The antenna is implemented on a low-loss substrate and evaluated using full-wave electromagnetic simulations to assess impedance matching, radiation performance, and MIMO diversity metrics. To enhance inter-port isolation in the array, an inverted U-shaped defected ground structure (DGS) is introduced between the two radiating elements. The optimized design achieves excellent matching around 2.4 GHz and ultra-high isolation of approximately -78.7 dB, while maintaining stable gain and radiation patterns across the operating band. These results indicate that the proposed antenna offers a simple and effective solution for compact, energy-efficient, and robust 2.4 GHz MIMO front ends in internet of things (IoT) and other short-range wireless communication systems.

Corresponding Author:

Meriem Boucif
Department of Telecommunication, Laboratory of Telecommunication
Faculty of Technology, University of Tlemcen
Tlemcen, Algeria
Email: meriem.boucif@univ-tlemcen.dz

1. INTRODUCTION

The rapid growth of wireless communication systems operating in the 2.4 GHz industrial, scientific, and medical (ISM) band, including Wi-Fi and internet of things (IoT) platforms, has intensified the demand for compact antenna systems capable of supporting reliable multiple-input multiple-output (MIMO) links. Microstrip patch antennas (MPAs) are widely adopted in such devices because of their low profile, ease of integration, and cost-effectiveness [1]. However, when conventional single-element MPAs are arranged into closely spaced MIMO arrays, they often suffer from limited impedance bandwidth and insufficient inter-port isolation, which degrade diversity performance and overall link reliability [2].

Foundational electromagnetic models for patch analysis and design, such as the cavity model and dominant-mode synthesis, remain central to contemporary optimization workflows [3]. Building on these fundamentals, many recent MIMO antenna designs focus either on modifying the radiating elements using slots, parasitic resonators, or stubs to redistribute surface currents, or on engineering the ground plane through defected ground structures (DGS), partial grounds, or etching patterns to suppress surface waves and reduce mutual coupling [4]-[12].

Several representative designs illustrate these approaches across sub-6 GHz and millimeter-wave bands. Najim *et al.* [13] developed a four-element printed dipole MIMO antenna with 3.3-6.6 GHz

bandwidth and 5.2-7.05 dB gain. Wu *et al.* [14] employed circular stubs to decouple circular patches, achieving isolation up to -23.8 dB. Saleem *et al.* [15] used split-ring resonator (SRR) loading to obtain ultra-wideband operation with coupling suppression below -20 dB. Subashini *et al.* [16] targeted 28 GHz circular MIMO, while Singh *et al.* [17] reported about -16 dB isolation in a sub-6 GHz circular array. In most of these compact layouts, isolation typically remains within the -16 dB to -25 dB range [13]-[17]. Achieving higher isolation often necessitates more complex decoupling circuits that increase the footprint or design complexity. This highlights the need for further enhancement using simple structures without compromising antenna size or efficiency.

Motivated by these limitations, this paper proposes a compact circular microstrip MIMO antenna for 2.4 GHz operation on Rogers RT5880 (ε_r = 2.2, tan δ = 0.0009) that employs a simple inverted U-shaped DGS etched between two circular radiators. The DGS is designed to disturb and reroute the ground-plane currents in the inter-element region, thereby weakening the dominant coupling paths while preserving the impedance behavior of each port. The antenna is analyzed using full-wave electromagnetic simulations in CST Microwave Studio, with one port excited and the other terminated in 50 Ω, to assess matching, isolation, radiation performance and standard MIMO diversity metrics.

The main contributions of this work can be summarized as follows. First, a dual-port circular patch configuration is introduced that achieves very high inter-port isolation using only a single inverted U-shaped DGS on the common ground plane, without relying on neutralization lines, EBG superstrates or lumped decoupling networks. Second, the proposed layout maintains good impedance matching and stable radiation patterns despite the close spacing between elements, making it attractive for compact 2.4 GHz front ends. Third, a comprehensive MIMO performance evaluation is carried out, including S-parameters, input matching, radiation characteristics and envelope correlation/diversity gain analysis, which clarifies the physical decoupling mechanism associated with the DGS and quantifies its impact on system-level metrics. It is further noted that all results reported in this paper are obtained from full-wave electromagnetic simulations; experimental validation on a fabricated prototype is left for future work.

The remainder of this paper is organized as follows. Section 2 describes the antenna configuration and design methodology, including the single-element circular patch, the extension to the two-port MIMO layout and the geometry of the inverted U-shaped DGS. Section 3 presents and discusses simulation results, covering impedance bandwidth, isolation, radiation patterns, diversity performance and comparison with related works. Section 4 concludes the paper and outlines directions for future research.

2. METHOD

2.1. Antenna design theory

The circular microstrip radiator was sized using the classical cavity-model formulation [3]. A common starting estimate for the physical patch radius, which accounts for fringing fields, is expressed as:

$$a = \frac{F}{\sqrt{1+\frac{2h}{\pi\varepsilon_r F}\left(ln\left(\frac{\pi F}{2h}\right)+1.7726\right)}} \quad (1)$$

With,

$$F = \frac{8.791\times10^9}{f_{r\sqrt{\varepsilon_r}}} \quad (2)$$

Here, f_r is the target resonance frequency (2.4 GHz), ε_r is the substrate relative permittivity (2.2 for Rogers RT5880), and h is the substrate thickness (1.6 mm). A refined estimate for the effective radius a_e, which captures fringing effects more accurately, is given by:

$$a_e = a\left[1+\frac{2h}{\pi a\varepsilon_r}\left(\ln\left(\frac{\pi a}{2h}\right)+1.7726\right)\right]^{\frac{1}{2}} \quad (3)$$

The dominant TM_{11} resonance can then be approximated as:

$$f_{r,TM_{11}} \approx \frac{X'_{11}\,c}{2\pi\,a_e\sqrt{\varepsilon_{eff}}} \quad (4)$$

where c is the speed of light and ε_{eff} is the effective permittivity (for thin substrates, $\varepsilon_{eff} \approx \frac{\varepsilon_{r+1}}{2}$ is often a good estimate) and X'_{11} is the first root for the TM_{11} mode.

In this work, Rogers RT5880 was selected ($\varepsilon_r = 2.2$, $tan\delta = 0.0009$) with $h = 1.6\,mm$ at $f_r = 2.4\,GHz$. In (1)-(3) yield an initial estimate of the circular patch radius of 23.62 mm. After full-wave

optimization in CST Microwave Studio, the single-element design was finalized at $a = 23.66\,mm$. During two-element MIMO co-optimization, which accounted for the inverted U-shaped defected ground structure (DGS) and inter-element coupling, the radius converged to $a = 23.71\,mm$. These adjustments are small ($\leq$ 0.21 %) and reflect the expected fine-tuning once the feed and coupling environment are included.

The metallization (patch and ground plane) used standard copper thickness $t = 0.035\,mm$. Following Balanis' conservative guideline of extending the ground plane by $6h$ beyond the patch on each side, the ground size for the single-element case was:

$$L_g = W_g = 2a + 12h \tag{5}$$

With $a = 23.66\,mm$ and $h = 1.6\,mm$, this gives $L_g = W_g = 66.52\,mm$. For more compact layouts, the milder recommendation $L_g = W_g = 2a + 6h$ is often adopted; with the same a and h this yields 56.92 mm, which was the value retained here to save area while still providing sufficient clearance for the coaxial connector and mitigating edge diffraction.

2.2. Feeding mechanism

The antenna was fed by a 50 Ω coaxial probe with PTFE dielectric. The outer and inner conductor diameters are $D = 4.5\,mm$ and $d = 1.26\,mm$, respectively. The feed position was empirically optimized in CST Microwave Studio to minimize the input mismatch at 2.4 GHz for the single-element configuration. The final in-plane offset from the patch center was $(x_f, y_f = 6\,mm, 6\,mm)$, with radial distance.

$$r_f = \sqrt{x_f^2 + y_f^2} \approx 8.49\,mm \tag{6}$$

This location produced excellent impedance matching. For circular patches, the feed can be placed at any azimuth for the same radial distance r_f; in this design, a first-quadrant point was chosen for practical routing convenience. In the MIMO configuration, the coaxial feed of each element was slightly shifted to $(x_f, y_f = 6.2\,mm, 5\,mm)$, to compensate for the effect of inter-element coupling.

2.3. Single-element model

The single antenna element was designed and modelled in CST Microwave Studio using a Rogers RT5880 substrate with relative permittivity $\varepsilon_r = 2.2$, loss tangent, $tan\delta = 0.0009$, and thickness $h = 1.6\,mm$. Both the patch and ground plane were realized with copper metallization of thickness $t = 0.035mm$, while the ground plane dimensions were set to $L_g = W_g = 56.92mm$. Open (add space) boundary conditions were applied, and a hexahedral mesh with adaptive refinement was employed to ensure simulation accuracy. No hardware prototype was fabricated at this stage; all performance metrics reported in this paper are obtained from full-wave electromagnetic simulations.

All key design parameters, including patch radius, feed locations, DGS dimensions, and substrate properties, are explicitly reported to enable straightforward reproduction of the antenna geometry and simulation setup. The optimized design provided excellent impedance matching and stable radiation performance at the target frequency of 2.4 GHz. The overall geometry and design parameters of the circular patch antenna are shown in Figure 1.

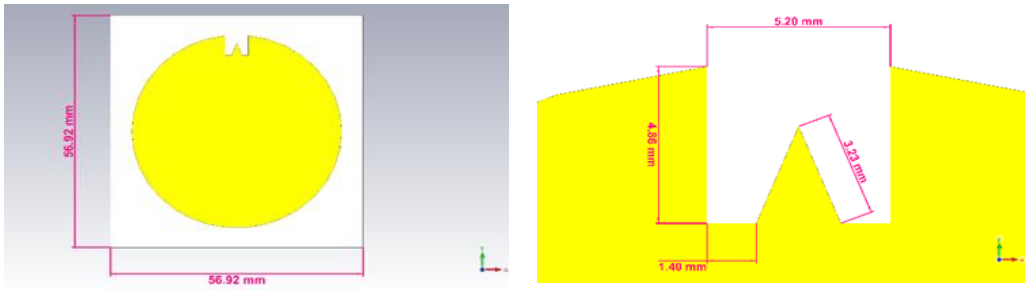

Figure 1. Geometry of the circular patch antenna with design parameters

2.4. Two-element MIMO layout with inverted U-Shaped DGS

Figure 2 illustrates the geometry of the proposed two-element circular MIMO antenna with an inverted U-shaped defected ground structure (DGS). The antenna consists of two identical circular patches arranged on the same substrate and excited using coaxial feeds.

To extend the design into a two-element MIMO configuration, the two circular patches were arranged with an edge-to-edge separation $D_{sep} = 64\,mm \approx 0.5\,\lambda_0$ and a center-to-center spacing $D_{cc} = 111.42$ mm $\approx 0.89\lambda_0$, as shown in Figure 2(a). These distances were chosen to maintain compactness while limiting near-field interaction. In the absence of additional isolation techniques, significant mutual coupling was observed, primarily caused by surface-wave propagation within the substrate.

To suppress this effect, an inverted U-shaped DGS was introduced in the common ground plane between the two radiators, as shown in Figure 2(b). This DGS perturbs the surface current distribution in the inter-element region, thereby interrupting the dominant coupling paths and enhancing inter-port isolation.

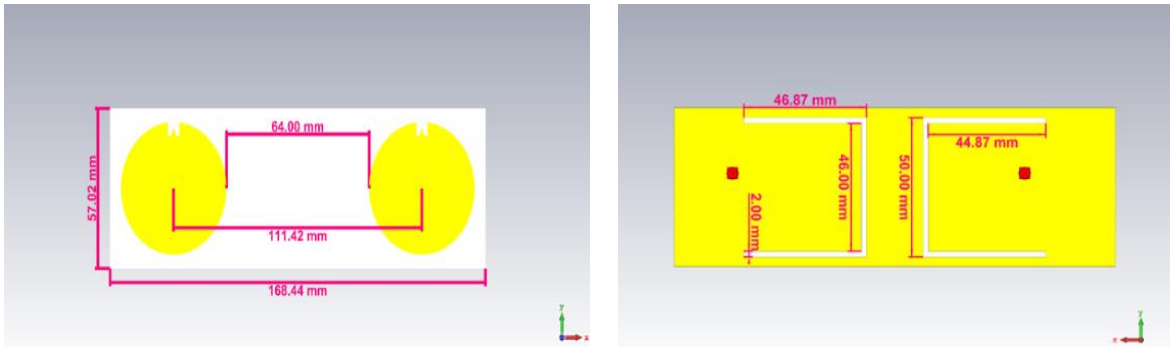

(a) (b)

Figure 2. Geometry of the two-element circular MIMO antenna (a) top view with the edge-to-edge separation D_{sep} and centre-to-centre spacing D_{cc} indicated between the two patches and (b) bottom view highlighting the inverted U-shaped defected ground structure (DGS) and the coaxial feed locations

3. RESULTS AND DISCUSSION

3.1. Single-element performance

The simulated reflection coefficient confirms the strong impedance performance of the single circular patch antenna. At 2.4 GHz, the radiator exhibits a deep resonance with a minimum $S_{11} = -44.54\,dB$ Figure 3. The corresponding voltage standing wave ratio (VSWR) is 1.01 Figure 4, which demonstrates nearly perfect matching to the 50 Ω reference impedance. The input impedance on the Smith chart is located very close to the 50 Ω point, with a negligible reactive component Figure 5. Consequently, reflections at the feed port are practically eliminated and almost all the input power is effectively delivered to the radiator.

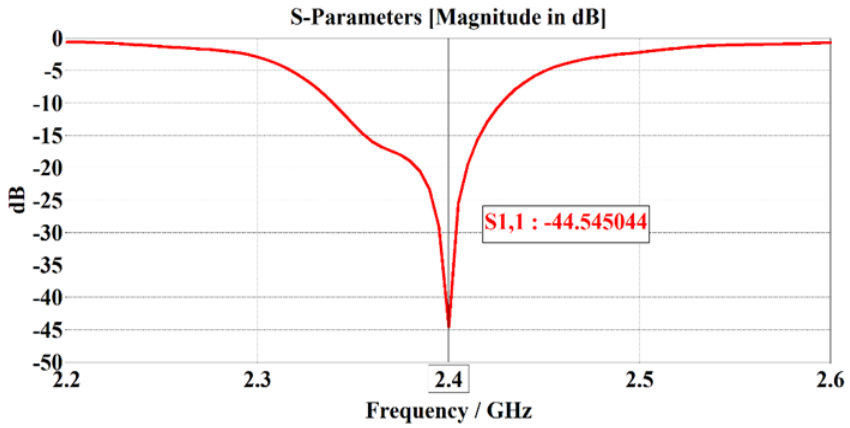

Figure 3. Simulated reflection coefficient of the single-element circular patch antenna at 2.4 GHz

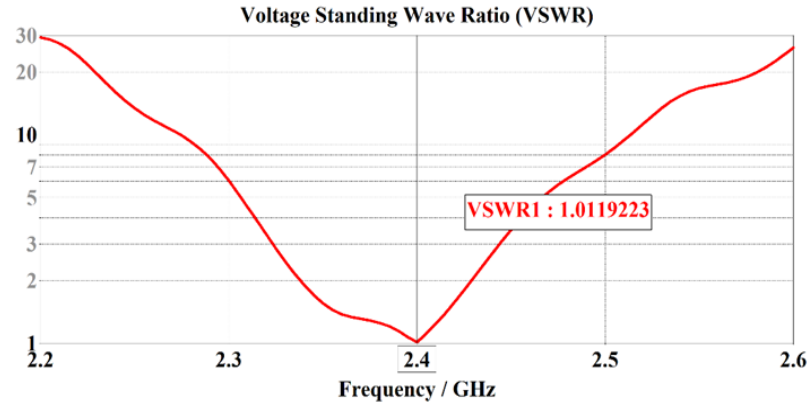

Figure 4. Simulated VSWR of the single antenna across the operating band

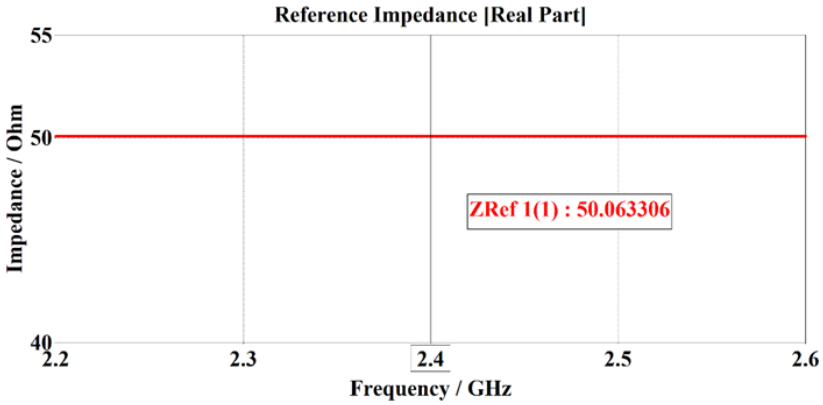

Figure 5. Simulated input impedance of the single antenna at 2.4 GHz

Radiation performance is similarly stable across the operating band. At 2.4 GHz, the antenna achieves a realized gain of 6.78 dBi Figure 6 and a directivity of 7.11 dBi Figure 6. The small difference between these two values indicates high radiation efficiency, since only a minimal portion of power is lost due to dielectric and ohmic dissipation. These results confirm that the single element provides a robust baseline for extension to a multi-port configuration.

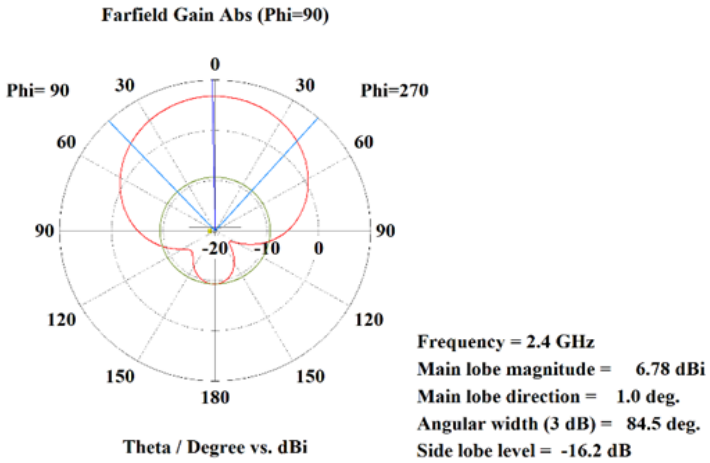

Figure 6. Simulated peak gain of the single antenna at 2.4 GHz

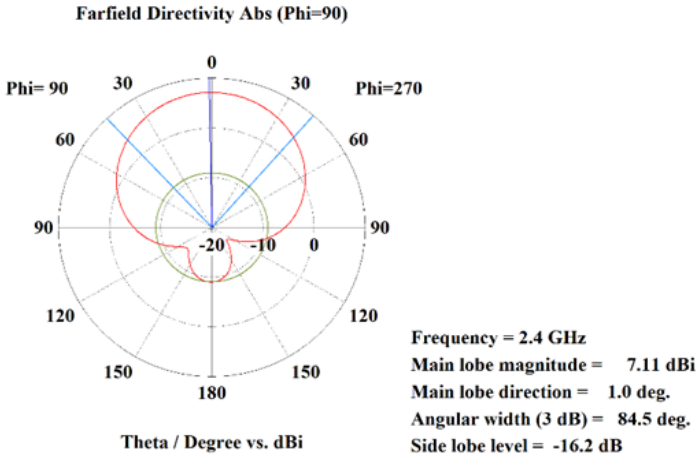

Figure 7. Simulated directivity pattern of the single antenna at 2.4 GHz

3.2. MIMO performance

The simulated input reflection coefficient demonstrates that the proposed two-element array maintains good impedance characteristics once integrated into the MIMO configuration. At 2.4 GHz, the antenna exhibits $S_{11} = -21.01\ dB$ when one port is excited and the other is terminated with a 50 Ω load Figure 8. The −10 dB impedance bandwidth extracted from $|S_{11}|$ spans 2.3277–2.4232 GHz, yielding BW = 95.5 MHz Figure 9. Within this band, the input impedance and VSWR responses, Figure 10 and Figure 11 confirm that the introduction of the inverted U-shaped DGS does not cause detrimental detuning. The array preserves a VSWR of about 1.2 at 2.4 GHz, ensuring stable matching for both ports and indicating that the isolation enhancement is achieved without sacrificing input adaptation.

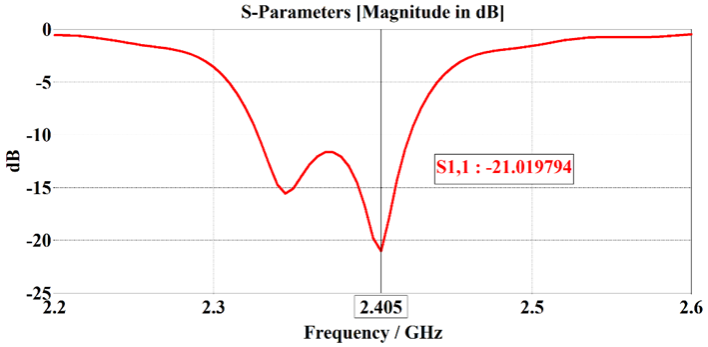

Figure 8. Simulated reflection coefficient S_{11} of the MIMO antenna with DGS

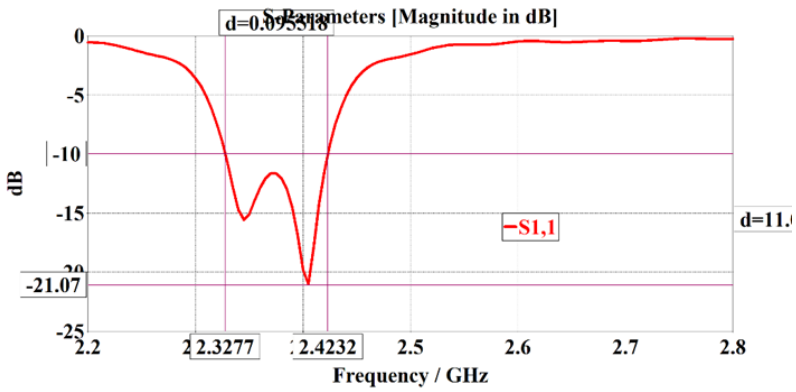

Figure 9. −10 dB Impedance Bandwidth of the Proposed Antenna (|S11|)

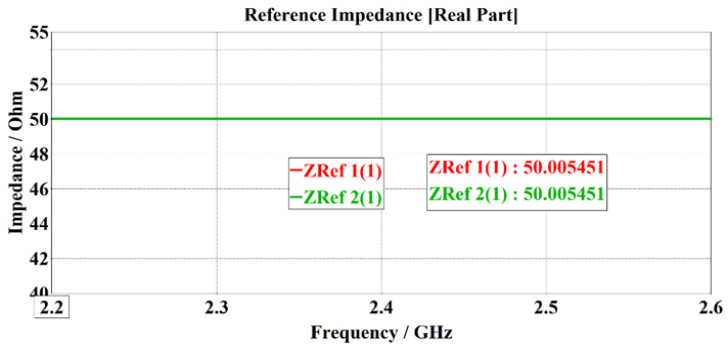

Figure 10. Simulated input impedance of the two-element MIMO antenna at 2.4 GHz

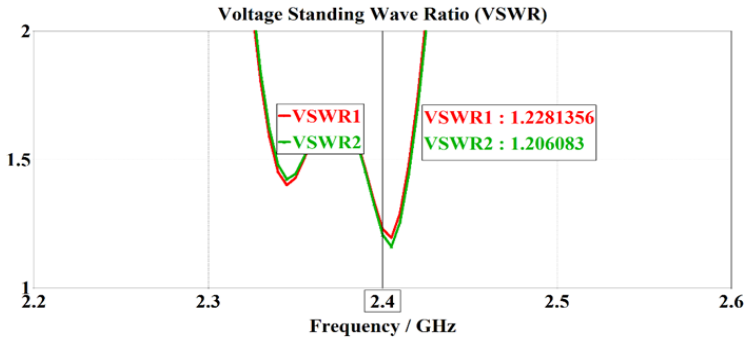

Figure 11. Simulated VSWR of both ports of the MIMO antenna at 2.4 GHz

Figure 12 presents the simulated transmission coefficient $|S_{21}|$ between the two ports for the reference two-element circular array without DGS and for the proposed configuration with the inverted U-shaped DGS. As a reference, the inter-port isolation of the same two-element circular array without the DGS was first evaluated. In this baseline configuration, the simulated transmission coefficient $|S_{21}|$ at 2.4 GHz is only about −27.52 dB, as shown in Figure 12(a), which is consistent with typical values reported for compact MIMO layouts without dedicated decoupling structures. This limited isolation confirms that additional measures are required to effectively suppress mutual coupling between the two patches.

A major outcome of the proposed layout is the dramatic improvement in inter-port isolation obtained after introducing the inverted U-shaped DGS. When the DGS is etched in the common ground plane between the two patches, the simulated transmission coefficient $|S_{21}|$drops to −78.65 dB at 2.4 GHz, as shown in Figure 12(b). By comparing Figure 12(a) and Figure 12(b), it is evident that the DGS provides a very strong suppression of mutual coupling, improving the isolation by more than −27.52 dB at the operating frequency. To the best of our knowledge, this isolation level significantly surpasses most reported values for compact dual-port antennas. Importantly, it is achieved without relying on neutralization lines, electromagnetic bandgap (EBG) superstrates, or additional lumped decoupling networks.

The radiation characteristics remain largely unaffected by the isolation enhancement. The MIMO configuration delivers a realized gain of 6.52 dBi and a directivity of 7.07 dBi at 2.4 GHz Figure 13 and Figure 14. The small separation between these values again indicates high radiation efficiency, suggesting that the DGS primarily mitigates surface-wave coupling while preserving the intrinsic aperture radiation of the patches. This behavior is consistent with the design objective of improving isolation without compromising gain or radiation patterns.

The surface-current distribution at 2.4 GHz Figure 15 clarifies the physical isolation mechanism. With Port 1 excited and Port 2 terminated in 50 Ω, the inverted U-shaped DGS confines strong currents around the excited radiator and along the slot edges, while significantly suppressing currents in the inter-element region and on the idle patch. This disruption of dominant ground-return paths is consistent with the very small $|S_{21}|$ observed at 2.4 GHz and underpins the excellent diversity metrics reported below. All these results are obtained from full-wave electromagnetic simulations; experimental validation on a fabricated prototype is left for future work and may introduce small deviations due to manufacturing tolerances and connector effects.

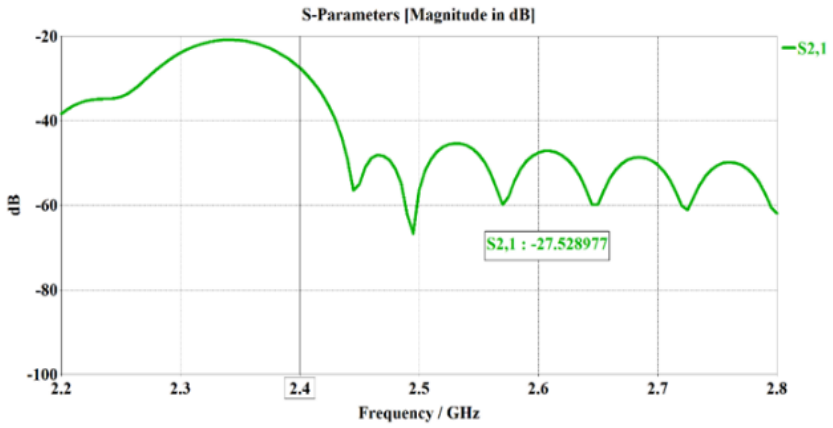

(a)

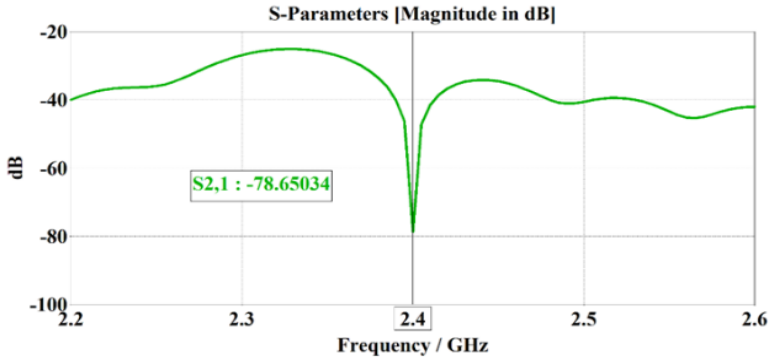

(b)

Figure 12. Simulated transmission coefficient S_{21} between the two ports: (a) reference two-element circular array without DGS, showing limited isolation at 2.4 GHz and (b) proposed array with inverted U-shaped DGS, demonstrating the achieved isolation enhancement at 2.4 GHz

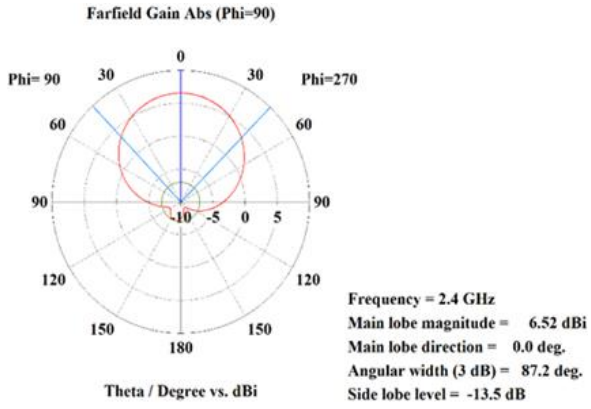

Figure 13. Simulated peak gain of the MIMO antenna

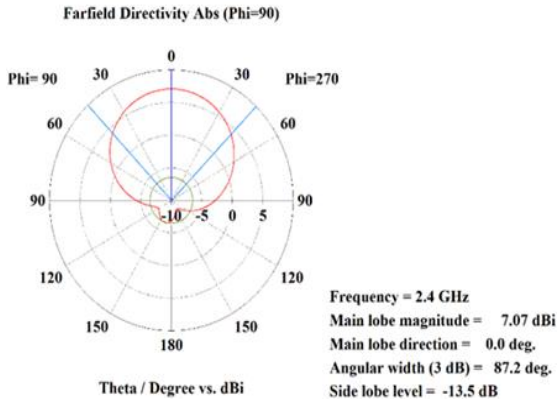

Figure 14. Simulated directivity pattern of the MIMO antenna

The diversity performance was evaluated using the envelope correlation coefficient (ECC) and the diversity gain (DG). As shown in Figure 16, the ECC remains extremely low around 2.4 GHz ($\approx 2.8 \times 10^{-7}$), which is several orders of magnitude below common MIMO thresholds such as 0.5 and even 0.1. This confirms excellent pattern and port diversity. The corresponding DG was obtained from the ECC using the standard relation.

$$DG = 10\sqrt{1 - ECC^2} \quad (7)$$

yielding DG ≈ 9.9999986 dB, essentially equal to the theoretical maximum of 10 dB Figure 17. The ECC was computed from the two-port scattering parameters using the formulation of Blanch *et al.* [18]. Together, these metrics show that the proposed antenna behaves as an almost ideal two-branch diversity system in the 2.4 GHz band.

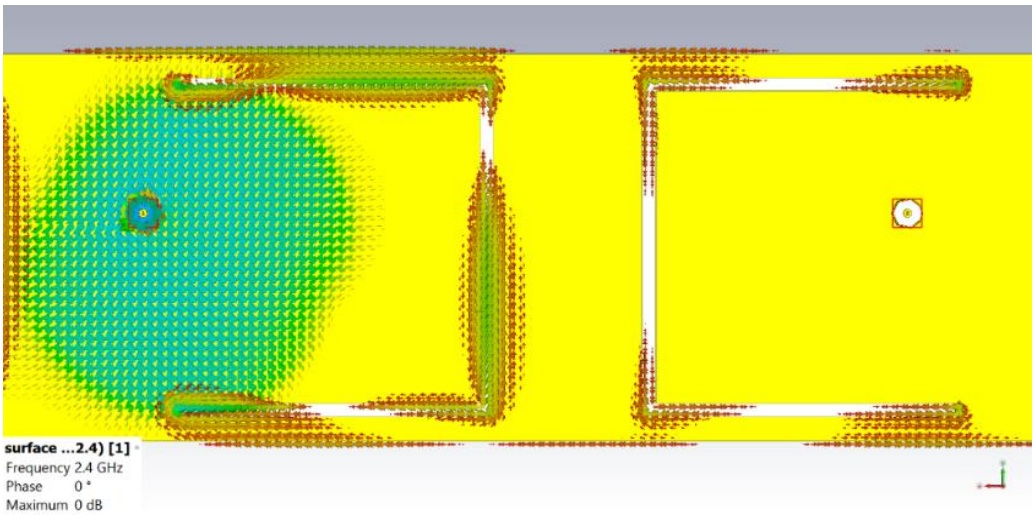

Figure 15. Surface current distribution at 2.4 GHz (bottom view, ground plane) with Port 1 excited and Port 2 terminated in 50 Ω, showing current confinement along the inverted U-shaped DGS and suppressed current on the idle element

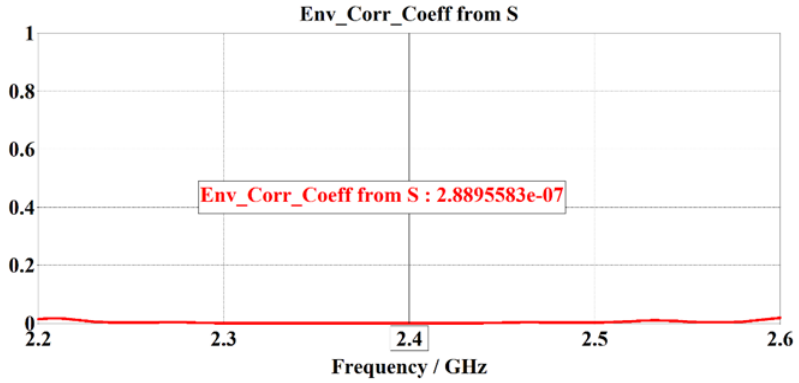

Figure 16. Simulated envelope correlation coefficient (ECC) for the proposed two-port MIMO antenna

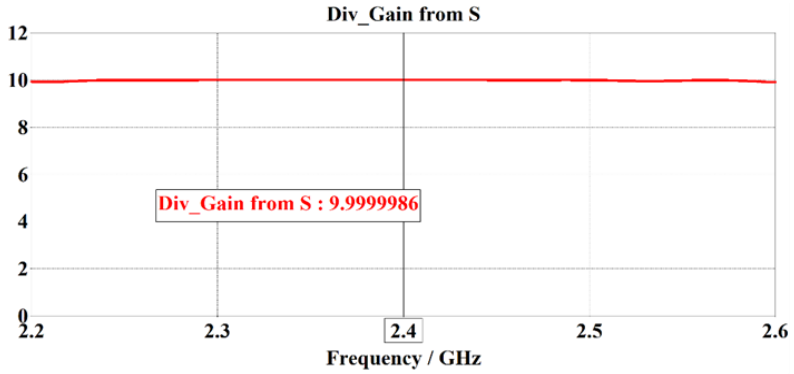

Figure 17. Simulated diversity gain (DG) for the proposed two-port MIMO antenna

3.3. Comparison with reported work

Table 1 benchmarks the proposed antenna against recent multi-port circular-patch MIMO designs operating from sub-6 GHz to millimetre-wave frequencies. The most salient outcome is isolation. The present design attains −78.65 dB at 2.4 GHz, which exceeds all listed peers by a wide margin. Reconfigurable sub-6 GHz designs such as [19] report −14.5 to −18 dB, and EBG/DGS-assisted CPW structures like [20] reach ≤ −35 dB (up to −47 dB in a special OFF state), while neutralization-line decoupling in [21] achieves isolation better than −60 dB in higher bands (3.2–4.14 GHz). Metasurface-integrated CP MIMO in [22] (5–8.67 GHz) and the integrated 8-port platform in [23] provide ≤ −22 dB and ≈ −26 dB isolation, respectively. At 2.4 GHz, the 4-port swastika-ground design in [24] reports −12.3 dB adjacent isolation, highlighting the challenge of strong decoupling near ISM frequencies. Collectively, these comparisons indicate that the inverted U-shaped DGS in this work provides a more effective and compact decoupling mechanism at 2.4 GHz than EBG, CP metasurfaces, or orientation-based self-decoupling techniques used elsewhere.

Beyond isolation, the proposed antenna sustains near-ideal diversity performance. The ECC ≈ 2.8×10^{-7} is orders of magnitude lower than commonly accepted limits (0.5 and 0.1) and even lower than the already excellent values reported in [20] (< 0.02) and [22] (< 0.005). Consistently, the DG ≈ 10 dB matches the theoretical maximum and is on par with high-quality MIMO references such as [19], [22], and [23].

In terms of radiation performance, the proposed design delivers a realized gain of about 6.5 dBi at 2.4 GHz together with an efficiency of approximately 92.6 %, estimated from the gain-to-directivity ratio. This is competitive with sub-6 GHz entries and notably higher than typical reconfigurable FR-4-based designs (e.g. [19], 65–75 %).

Finally, the functional scope differs across works. Reference [20] provides dual-band operation with very good isolation [23] scales to eight ports covering both sub-6 GHz and mm-wave bands, and [22] achieves circular polarization over a wide band via a metasurface. In contrast, the present work focuses on a single-band 2.4 GHz solution optimized for ultra-high isolation with minimal structural complexity, which is particularly attractive for IoT and ISM-band devices where robust co-existence and energy efficiency are critical. The trade-off is the single-band nature of the current design; however, the demonstrated DGS approach is structurally simple and amenable to future dual-band or multiband extensions.

Table 1. Performance comparison of reported multi-port antennas and the proposed design

Ref	Antenna type/structure	Ports	Freq. Band (s) (GHz)	Isolation (dB)	Gain (dBi)	DG (dB)	ECC	Eff. (%)
[19]	Reconfigurable circular-patch MIMO (inverted L-stubs + rectangular ground stub, FR-4)	2	3.3–3.99 / 4.96–5.34	−14.5 to −18	2.5 at 3.5 GHz; 2.68 at 5.1 GHz	9.9	< 0.09	65 / 75
[20]	Dual-band CPW circular-patch MIMO with PGP-DGS, PIN branch-lines, dual-band EBG	2	2.8–3.6 / 4.7–5.6 (ON); 5.2 (OFF)	≤ −35 (low), ≤ −25 (high); −47 at 5.2 GHz (OFF)	> 3 (low), > 4 (high ON), ≈ 3.5 (OFF)	—	—	—
[21]	Dual-band H-slotted circular patch + neutralization line (FR-4)	2	3.20–3.40 / 3.84–4.14	< −60 (meas.)	≳ 7	—	< 0.02	—
[22]	Dual-port bi-directional CP metasurface-integrated (FR-4, two layers)	2	5–8.67	≤ −22 (meas.)	6.5 / 6.55 dBic	> 9.985	< 0.005	> 80
[23]	Integrated 8-port: 4 CPW elliptical (sub-6) + 4 semi-circular (mm-wave) (FR-4)	8	3.20–5.50 / 23.50–29.95 (meas.)	≤ −25.5 / ≤ −25.95	12.3 / 10.55	9.99	0.002	86–91.8 / 89–96
[24]	4-port circular/slot, swastika-shaped ground (FR-4, 40×40×1.6 mm³)	4	2.4	−12.3	—	~10	—	> 85
[25]	2×2 CP MIMO circular notched patch (FR-4)	4	4.9–5.1	> 20	—	—	—	—
This work	Dual-port circular microstrip patch on Rogers RT5880 with inverted U-shaped DGS	2	2.4	−78.65	≈6.5	~10	≈ 2.8×10^{-7}	92.6

Key takeaway: at 2.4 GHz, the proposed antenna provides state-of-the-art isolation (−78.65 dB) with almost-zero ECC and high efficiency, outperforming comparable sub-6 GHz MIMO designs in decoupling effectiveness while maintaining competitive gain and near-ideal diversity performance.

While the isolation and diversity performance of the proposed antenna are outstanding, the present study is subject to several limitations. First, all results are based on CST Microwave Studio simulations, and fabrication tolerances, connector effects, and measurement uncertainties may slightly degrade the isolation

and radiation characteristics in practice. Second, the design is restricted to a single 2.4 GHz band, whereas many modern IoT and Wi-Fi devices operate over multiple bands. Third, mutual coupling has been evaluated in a free-space environment; performance in realistic deployments with device housings and nearby objects may differ. These limitations suggest clear directions for future work, including prototype fabrication and measurement in anechoic chambers, robustness analysis under manufacturing deviations, and extension of the DGS concept to dual-band or multiband circular MIMO arrays.

4. CONCLUSION AND FUTURE WORK

The aim of this study was to design and evaluate a circular microstrip patch antenna and its extension into a two-element MIMO configuration with very high inter-port isolation at 2.4 GHz. A single radiating element implemented on a Rogers RT5880 substrate exhibited excellent impedance matching, with low return loss, a near-ideal voltage standing-wave ratio (VSWR), and stable radiation characteristics. To improve isolation in the MIMO configuration, an inverted U-shaped defected ground structure (DGS) was introduced in the common ground plane between the two circular patches. The resulting dual-port antenna achieved an outstanding isolation level of approximately −78.65 dB at 2.4 GHz, while maintaining a realized gain of about 6.5 dBi, a directivity close to 7 dBi, and an envelope correlation coefficient that is essentially zero, corresponding to a diversity gain near 10 dB. These findings indicate that the proposed DGS-based layout provides a simple and effective means of strongly reducing mutual coupling in compact MIMO antennas without degrading impedance or radiation performance, thereby contributing to the design of robust 2.4 GHz front ends for ISM and IoT applications. The results reported in this work were obtained from full-wave electromagnetic simulations only; experimental validation has not yet been performed. Fabrication tolerances, connector effects, and practical deployment environments may slightly affect the measured isolation and radiation characteristics. Future research will therefore focus on prototype fabrication and measurement of the proposed antenna, as well as on extending the concept to dual-band or multiband operation and to larger MIMO arrays. These developments could further enhance the applicability of the design to next-generation wireless systems. We encourage subsequent studies to cite and build upon this work rather than reproducing its content verbatim, so that the proposed approach is properly referenced within the broader literature. Overall, the proposed dual-port circular patch antenna provides a practically attractive and structurally simple solution for achieving ultra-high isolation and near-ideal diversity performance at 2.4 GHz, and the DGS-based decoupling concept offers a solid foundation for subsequent designs that further extend its bandwidth, number of ports and application scope.

FUNDING INFORMATION

The authors state that no funding was involved in this research.

AUTHOR CONTRIBUTIONS STATEMENT

This journal applies the Contributor Roles Taxonomy (CRediT) to acknowledge individual author contributions. The contributions of each author are detailed below.

Name of Author	C	M	So	Va	Fo	I	R	D	O	E	Vi	Su	P	Fu
Meriem Boucif	✓	✓	✓	✓	✓	✓		✓	✓	✓	✓			
Fayza Bousalah										✓		✓	✓	
Hayat Benosman										✓		✓	✓	

C : **C**onceptualization
M : **M**ethodology
So : **So**ftware
Va : **Va**lidation
Fo : **Fo**rmal analysis
I : **I**nvestigation
R : **R**esources
D : **D**ata Curation
O : Writing - **O**riginal Draft
E : Writing - Review & **E**diting
Vi : **Vi**sualization
Su : **Su**pervision
P : **P**roject administration
Fu : **Fu**nding acquisition

CONFLICT OF INTEREST STATEMENT

The authors declare that they have no known competing financial interests or personal relationships that could have appeared to influence the work reported in this paper.

DATA AVAILABILITY

The authors confirm that the data supporting the findings of this study are available within the article.

REFERENCES

[1] L. Wang, C. X. Zhang, S. S. Xing, Y. H. Xu, W. B. Kong, and J. Shi, "A low-profile shared-aperture patch antenna with 2-D scanning capability," *IEEE Antennas and Wireless Propagation Letters*, vol. 24, no. 9, pp. 2974-2978, Sep. 2025, doi: 10.1109/LAWP.2025.3578513.

[2] H. Wang, Q. Zheng, Q. Li, and X. X. Yang, "Isolation improvement and bandwidth enhancement of dual-band MIMO antenna based on metamaterial wall," *IEEE Antennas and Wireless Propagation Letters*, vol. 24, no. 5, pp. 1144-1148, May 2025, doi: 10.1109/LAWP.2025.3527688.

[3] C. A. Balanis, *Antenna theory: analysis and design*. John wiley & sons, 2016.

[4] S. Gundala, V. Srinivasa Baba, S. Srigada, N. Pooja, K. Preethililly, and S. K. Talusani, "Cross slotted antenna at X band for wireless applications," in *2024 IEEE Wireless Antenna and Microwave Symposium, WAMS 2024*, IEEE, Feb. 2024, pp. 1-7. doi: 10.1109/WAMS59642.2024.10527953.

[5] R. W. Abd-Elsalam, H. E. Seleem, M. M. Abd-Elnaby, and A. H. Hussein, "Low SAR compact wideband/dual-band semicircular slot antenna structures for sub-6 GHz 5G wireless applications," *Eurasip Journal on Wireless Communications and Networking*, vol. 2025, no. 1, p. 3, Jan. 2025, doi: 10.1186/s13638-024-02424-x.

[6] M. Taraji, E. Baladi, and M. A. Antoniades, "Compact wideband and high gain horn slot antenna array fed by printed ridge gap waveguide for X band applications," *Scientific Reports*, vol. 15, no. 1, p. 17627, May 2025, doi: 10.1038/s41598-025-99482-y.

[7] L. C. Paul *et al.*, "A compact wrench-shaped patch antenna with a slotted parasitic element and semi-circular ground plane for 5G communication," *e-Prime - Advances in Electrical Engineering, Electronics and Energy*, vol. 6, p. 100334, Dec. 2023, doi: 10.1016/j.prime.2023.100334.

[8] L. C. Paul *et al.*, "A low-profile antenna with parasitic elements and a DGS-based partial ground plane for 5G/WMAN applications," *Discover Applied Sciences*, vol. 6, no. 1, p. 22, Jan. 2024, doi: 10.1007/s42452-024-05669-9.

[9] K. Karthika and K. Kavitha, "Design and development of parasitic elements loaded quadband frequency and pattern reconfigurable antenna," *International Journal of RF and Microwave Computer-Aided Engineering*, vol. 2023, pp. 1-10, May 2023, doi: 10.1155/2023/4034241.

[10] D. K. Choudhary, "A low-profile antenna design with defected ground structure for wireless networks," *Wireless Personal Communications*, pp. 1-12, Dec. 2025, doi: 10.1007/s11277-025-11884-3

[11] A. H. Harkare, A. G. Kothari, A. A. Bhurane, Y. Solunke, and P. Peshwe, "Axial ratio and impedance bandwidth enhancement of a circularly polarized dielectric resonator antenna using defected ground structure," *Microwave and Optical Technology Letters*, vol. 67, no. 2, Feb. 2025, doi: 10.1002/mop.70140.

[12] R. H. Elabd, A. J. A. Al-Gburi, and A. A. Megahed, "Compact circular MIMO antenna with defected ground structure (DGS) for improved isolation in 5G sub-6GHz mobile systems," *Results in Engineering*, vol. 27, p. 105737, Sep. 2025, doi: 10.1016/j.rineng.2025.105737.

[13] H. S. Najim, M. F. Mosleh, and R. A. Abd-Alhameed, "Design a MIMO printed dipole antenna for 5G sub-band applications," *Indonesian Journal of Electrical Engineering and Computer Science (IJEECS)*, vol. 27, no. 3, pp. 1649-1660, Sep. 2022, doi: 10.11591/ijeecs.v27.i3.pp1649-1660.

[14] Z. Wu, L. Li, Y. Xiao, and S. R. Xie, "A Simple decoupling method for closely-spaced circular patch antennas," in *2024 IEEE MTT-S International Wireless Symposium, IWS 2024 - Proceedings*, IEEE, May 2024, pp. 1-3. doi: 10.1109/IWS61525.2024.10713804.

[15] S. Saleem, S. Kumari, V. Mirdha, D. Yadav, and D. Bhatnagar, "Circular split ring resonator (SRR) slot and ground stub based slotted circular ultra-wideband MIMO antenna with WLAN band exclusion and high isolation performance," *Sadhana*, vol. 49, no. 1, p. 26, Jan. 2024, doi: 10.1007/s12046-023-02356-0.

[16] V. Subashini, S. Aasitha, V. Brindha, K. Madhumitaa, and B. Rajalakshmi, "Design of circular-shaped two-element MIMO antenna for 5G communication," in *2024 International Conference on Communication, Computing and Internet of Things, IC3IoT 2024 - Proceedings*, IEEE, Apr. 2024, pp. 1-5. doi: 10.1109/IC3IoT60841.2024.10550339.

[17] A. K. Singh, S. K. Mahto, and R. Sinha, "Circular shape dual element mimo antenna for 5G (Sub-6GHz) application," in *2022 IEEE Microwaves, Antennas, and Propagation Conference, MAPCON 2022*, IEEE, Dec. 2022, pp. 583-587. doi: 10.1109/MAPCON56011.2022.10046871.

[18] S. Blanch, J. Romeu, and I. Corbella, "Exact representation of antenna system diversity performance from input parameter description," *Electronics Letters*, vol. 39, no. 9, pp. 705-707, May 2003, doi: 10.1049/el:20030495.

[19] A. K. Singh, S. K. Mahto, P. Kumar, R. K. Mistri, and R. Sinha, "Reconfigurable circular patch MIMO antenna for 5G (sub-6 GHz) and WLAN applications," *International Journal of Communication Systems*, vol. 35, no. 16, Nov. 2022, doi: 10.1002/dac.5313.

[20] P. B. Nikam, J. Kumar, V. Sivanagaraju, and A. Baidya, "Dual-band reconfigurable EBG loaded circular patch MIMO antenna using defected ground structure (DGS) and PIN diode integrated branch-lines (BLs)," *Measurement: Journal of the International Measurement Confederation*, vol. 195, p. 111127, May 2022, doi: 10.1016/j.measurement.2022.111127.

[21] R. L. Gali and M. Tatineni, "Design of a Dual-Band H-Cut circular antenna with various decoupling methods for 5G NR band," in *Proceedings of 8th International Conference on Inventive Computation Technologies, ICICT 2025*, IEEE, Apr. 2025, pp. 1935–1939. doi: 10.1109/ICICT64420.2025.11005281.

[22] P. Sritongnuan, P. Thitimahatthanakusol, N. Supreeyatitikul, and J. Konpang, "Dual-port bi-directional CP metasurface-integrated MIMO antenna for Wi-Fi 7 full-duplex communications," *Engineering Science and Technology, an International Journal*, vol. 68, p. 102103, Aug. 2025, doi: 10.1016/j.jestch.2025.102103.

[23] M. Srinubabu and N. V. Rajasekhar, "A compact and highly isolated integrated 8-port MIMO antenna for sub-6 GHz and mm-wave 5G-NR applications," *Results in Engineering*, vol. 25, p. 104068, Mar. 2025, doi: 10.1016/j.rineng.2025.104068.

[24] P. S. Chowdary and S. K. Panda, "Performance analysis of a swastika shaped MIMO antenna for wireless communication applications," *Engineering, Technology and Applied Science Research*, vol. 15, no. 1, pp. 19971-19976, Feb. 2025, doi: 10.48084/etasr.9478.

[25] R. Thommandru and R. Saravanakumar, "Cost-effective circularly polarized MIMO antenna for Wi-Fi applications," *Indonesian Journal of Electrical Engineering and Computer Science (IJEECS)*, vol. 36, no. 2, pp. 785-792, Nov. 2024, doi: 10.11591/ijeecs.v36.i2.pp785-792.

BIOGRAPHIES OF AUTHORS

Meriem Boucif was born in Tlemcen, Algeria, in 1996. She obtained her Baccalaureate degree in Natural Sciences in 2015, her Bachelor's degree in Telecommunications in 2018, and her Master's degree in Networks and Telecommunications in 2020, all from the University of Tlemcen. She is currently pursuing a Ph.D. degree in Telecommunications at the Department of Telecommunications, Faculty of Technology, University of Tlemcen. Her research interests include microstrip antennas, MIMO systems, and electromagnetic modeling. She can be contacted at email: meriem.boucif@univ-tlemcen.dz.

Fayza Bousalah was born in Tlemcen, Algeria, in 1982. She obtained her Bachelor's degree in Natural and Life Sciences in 2000, and in 2005 she received the State Engineer diploma in Telecommunications, specializing in Computer Science. She worked for nine years as a telecommunications and computer engineer for the Wilaya and Municipality of Tlemcen, while preparing her Magister and Doctoral theses in parallel. She received the Magister degree in Telecommunications in 2009 and the Ph.D. degree in Telecommunications in June 2015. In October 2015, she was appointed as a permanent faculty member in Telecommunications at the University Abou-Bekr Belkaid of Tlemcen, Algeria, where she currently serves as Assistant Professor in the Department of Telecommunications. Her research interests include wireless communications, antennas, and signal processing. She can be contacted at email: bousalah.fayza@univ-tlemcen.dz.

Hayat Benosman was born in Tlemcen, Algeria. She received the D.E.S. degree in Physics and the Magister degree in Physics with specialization in Electronics and Physical Modeling from the University of Tlemcen, Algeria. She obtained her Ph.D. degree in Telecommunications from the University of Tlemcen (UABT), Algeria, in 2014. Since 2015, she has been a faculty member in the Department of Telecommunications, University of Tlemcen. Her research interests include microwave engineering, antenna design, and wireless communication systems. She can be contacted at email: benosman.hayat@univ-tlemcen.dz.